Effects of indenter angle on micro-scale fracture toughness measurement by pillar splitting

Matteo Ghidelli, Marco Sebastiani, Kurt Johanns, George Pharr

Effects of indenter geometry on micro-scale fracture toughness measurement by pillar splitting

M. Ghidelli[1], M. Sebastiani[1], K. E. Johanns[2], G. M. Pharr[3]

[1] "Roma Tre" University, Engineering Department, Via della Vasca Navale 79, 00146, Rome, Italy

[2] Nanomechanics Inc., 105 Meco Ln, Oak Ridge, TN, 37830, USA

[3] Texas A&M University, Department of Materials Science & Engineering

Email: matteo.ghidelli@uniroma3.it, marco.sebastiani@uniroma3.it

Abstract

We present improvements to a recently developed pillar splitting technique that can be used to characterize the fracture toughness of materials at the micrometer scale. Micro-pillars with different aspect ratios were milled from bulk Si (100) and TiN and CrN thin films, and pillar splitting tests were carried out using four different triangular pyramidal indenters with centerline-to-face angles varying from 35.3° to 65.3°. Cohesive zone finite element modelling (CZ-FEM) was used to evaluate the effect of different material parameters and indenter geometries on the splitting behavior. Pillar splitting experiments revealed a linear relationship between the splitting load and the indenter angle, while CZ-FEM simulations provided the dimensionless coefficients needed to estimate the fracture toughness from the splitting load. The results provide novel insights into the fracture toughness of materials at small scales using the pillar spitting technique and provide a simple and reliable way to measure fracture toughness over a broad range of material properties.

I. Introduction

The need to develop new high-performance materials combined with continuing device miniaturization has pushed scientists to investigate the mechanical behavior of materials at smaller and smaller scales [1]. Sub micrometer-scaled materials in thin film form can exhibit mechanical properties that are significantly different from their bulk counterparts due to the influences of surface and interfacial effects in addition to microstructural changes [2]. In crystalline thin films, dislocation motion is often severely constrained by the presence of the substrate [2,3], while in thin metallic glass films, the nucleation and propagation of shear bands can be equally affected [2,4,5]. The net result of these effects is often an increase in apparent strength of the film relative to the bulk material [2-4]. These effects have led investigators to develop new tests that can assess the inherent mechanical properties of thin film materials independent of the substrate effects [2].

Among the numerous mechanical properties of interest, knowledge of the fracture toughness at the micrometer scale is of major importance in the design of devices such as micro-electro-mechanical-systems (MEMS) subjected to mechanical fatigue and wear-resistant thin films [1,6,7]. In the literature, several different methods have been proposed to measure the fracture toughness of small-scale materials, as summarized in recent review articles [6,7]. Vickers indentation cracking techniques were among the first proposed because of the ease of testing and sample preparation [8,9]. In such tests, a four-sided pyramidal indenter is used to generate radial cracks around the indentation impression [8,9], and the fracture toughness (K_c) is extracted by measuring the length of the cracks for a given maximum applied indentation load. Several models have been developed to estimate K_c depending on the indenter geometry and crack geometry, i.e. median, radial, half penny crack, cone or lateral cracks [10,11]. However, several important limitations exist in the application of these models to thin films [6,7]. First, the choice of the proper model requires a knowledge of the actual geometry of the crack, which has been demonstrated to be a function of the ratio of the elastic modulus to hardness (E/H),

Poisson's ratio and the indenter geometry [11]. Second, as the sample dimensions are decreased, the effect of the substrate can be enhanced by affecting the size and the development of the plastic zone under the indenter, which can influence the development of radial cracks from the hardness impression. Third, crack nucleation and propagation is strongly influenced by the presence of residual stresses, which can be high in thin ceramic films, thereby limiting the application of the method to films in which the residual stresses are accurately known by other techniques [6,7]. Lastly, the effects of the specimen microstructure such as the grain size distribution, the presence of secondary phases/precipitates, combined with the interface with the substrate further complicate the extraction of K_c for thin films [6,7].

To address these issues, a number of innovative techniques has been developed relying on fabrication by focused ion beam milling (FIB) of micro-beams deformed using a nanoindenter [6,7]. In these techniques, a crack propagates from a notch in the micro-specimen until failure, and an analytical model is used to extract the fracture toughness [6,7]. The main testing geometries are single [12-15] and double cantilever beams [16]. The single cantilever beam technique enables a measurement of the fracture toughness of the film material, while providing information about the adhesion as well [12-14]. Jaya *et al.* [15] successfully used this technique to extract the fracture toughness as a function of the temperature. However, the method is limited by the fact that the cantilevers have to be milled at the edge of the specimen in order to perform bending [12-14]. Furthermore, recent studies by Best *et al.* [17] showed that both the ion current during Ga+ milling and the type of FIB source (Ga^+, Xe^+, or He^+) have significant effects on the measured fracture toughness. In the double-cantilever geometry, the crack is propagated upon the application of a compressive load on specially designed specimens [16]. This technique does not have issues related to the edge positioning, but the measurements can affected by the geometry of the pre-notch, the FIB current used to fabricate specimens, and the friction between the indenter and the specimen [16]. It is also notable that the preparation of the specimens can be

affected by FIB milling damage, which can introduce free volume, chemical softening, and/or surface ion implantation, effects that are most notably enhanced for the thinnest specimens [6,7]. Furthermore, the presence of residual stresses can induce out-of-plane bending of single-cantilevers, while double cantilevers require an estimation of the friction coefficient between the indenter and the specimen. Lastly, cantilever bending techniques can be applied only to a small number of specimens due to the difficulty and time required for specimen preparation.

Recently, Sebastiani *et al.* [6,18] developed a pillar splitting technique in order to avoid some of these shortcomings. In this technique, FIB milling is used to fabricate cylindrical micro-pillars that are loaded to fracture by nanoindentation using a sharp pyramidal indenter [6,18]. The fracture toughness K_c is calculated from the splitting load (P_c), measured as the load at which a displacement burst is detected on the load-displacement curve, the pillar radius (R), and a coefficient γ determined from cohesive zone finite element modelling (CZ-FEM) through the relation

$$K_c = \gamma \frac{P_c}{R^{3/2}} \ . \qquad (1)$$

This method combines the advantages of the standard indentation cracking technique with the ease of application [6,18]. Moreover, a measurement of crack length is not required, and residual stresses are not an issue because they are completely released by the FIB milling process [6,18]. In addition, Best *et al.* [17] have suggested that the effects of ion damage are significantly reduced with respect to other techniques, since the crack nucleation and growth before instability occurs in the core of the pillar, where FIB damage is negligible. Pillar splitting has been recently validated for bulk silicon (100) and several ceramic thin films (TiN, CrN) and composites ($CrAlN/Si_3N_4$) [6,17,18]. It has also been used to estimate the fracture toughness for $Li_xMn_2O_4$ battery cathodes as a function of the state of charge [19].

To date, pillar-splitting fracture toughness measurements have been performed only using a Berkovich indenter and a fixed Poisson's ratio of 0.25, for which cohesive zone finite element

modeling (CZ-FEM) has been carried out to determine the coefficient γ in equation (1) [6,17,18]. For some materials, e.g., hard metals and intermetallics, splitting may not be achieved by the Berkovich indenter but could possibly be induced with a sharper indenter, e.g., a cube-corner indenter. To this end, here we extend the use of the pillar splitting technique to four different indenter geometries with angles ranging from 35.3° (cube-corner) up to 65.3° (Berkovich). Pillar splitting experiments with these indenters were performed on pillars with diameters ranging from 3 to 5 μm prepared from three different thin film materials - Si (100), TiN and CrN, and cohesive zone finite element modeling was used to determine the γ coefficients. We show that: (i) for a given material, the splitting load decreases linearly when with the indenter angle; (ii) the measured fracture toughness is not affected by the pillar diameter, provided that it is significantly higher than grain size; and (iii) there is a good agreement between the experiments and simulations.

II. Experimental details

Three materials were studied in this investigation: a bulk (100) single-crystal Si wafer, a 5 μm-thick TiN film, and a 3 μm-thick CrN film. The TiN film was deposited by cathodic arc physical vapor deposition (CAE-PVD), while magnetron sputtering PVD was used to deposit the CrN film [6,18]. The hardness and the elastic modulus of the specimen were measured by nanoindentation using a Keysight G200 Nanoindenter equipped with a diamond Berkovich tip. The measurements were carried out overnight using the continuous stiffness measurement (CSM) technique and a constant strain rate of 0.05 s^{-1}. The instrument frame stiffness and the indenter area function were calibrated before testing using a fused quartz reference sample. The hardness and the elastic modulus were extracted at a penetration depth at 100 nm to avoid surface and substrate effects.

All pillars were milled with a FIB-SEM (FEI Helios NanoLab 600) using an outer-to-inner single-pass with a two-step strategy. Beam currents of 48 pA and 12 pA were used for the preliminary

and final milling, respectively. Pillars with diameters of 5 μm and 3 μm were prepared, all with an aspect ratio (*z/D*) greater than 1.0, where z is the pillar height and *D* the top diameter. These dimensions assured complete relaxation of the film residual stress and minimal effects of substrate compliance during crack propagation [6,18]. The milling conditions enabled a precise geometry of the pillar with a minimal taper angle and negligible lateral ion damage [20].

Pillar splitting experiments were carried out with a Keysight G200 Nanoindenter using four different three-sided pyramidal diamond tips with centerline-to-face angles of to 35.3° (cube corner), 45°, 55° and 65.3° (Berkovich). Loading was controlled such that the loading rate divided by the load was constant and equal to 0.05 s^{-1} until unstable crack propagation was observed. To avoid complications caused by a small oscillating load, continuous stiffness measurement (CSM) was switched off during these experiments. After splitting, the pillars were imaged with an FEI Helios NanoLab 600 to verify centering of the indenter on the pillar and analyze splitting behavior.

Cohesive zone finite element modeling (CZ-FEM) was performed using ABAQUS-v6 in order to extract the γ coefficient in equation (1) and their variation with material properties. In all simulations, the aspect ratio of the pillar was 1.0. Details about the finite element modeling have been reported elsewhere [18]. The effects of the indenter geometry were examined over a range of *E/H* (ratio of the elastic modulus to hardness) from 5 to 30, while fixing Poisson ratio at 0.25. Influences of varying Poisson's ratio were examined for the Berkovich (65.3°) indenter with *E/H* ranging from 5 to 30.

III. Results and discussion

Figure 1 shows SEM micrographs of the micro-pillars before and after splitting. Before splitting, the pillars had a cylindrical shape with a small (< 2°) taper angle. The pillar diameters were 5 μm for the (100) Si, 3 μm for the CrN, and both 5 and 3 μm for the TiN. The SEM images after splitting show that the pillars were well-centered, even for the 3 μm pillars, for which the centering requires careful positioning. Evidence of the pillar centering for the sharper indenters is given by the indenter marks left outside the milling zone. For the pillars split with Berkovich and 55° tips, the failure occurred in 3 small pieces separated by approximatively 120° as imposed by the indenter pyramidal geometry [6,18]. For the sharper indenters (45° and cube corner), the pillars broke into 3 parts, often falling into the surrounding moat. This is because the large localized stress on a smaller contact area for sharper tips favors a large penetration after unstable splitting.

Figure 2a shows the load-depth curve for the Si (100) pillars for each of the four different indenter geometries along with a load-depth curve for Berkovich indentation in bulk Si. After an initial parabolic trend, a large displacement burst occurs indicating that the pillar has split. The splitting load varies as a function of the indenter geometry from 16.14 mN for the Berkovich tip down to 5.11 mN for the sharper cube-corner indenter. For the bulk material, the loading curve is well-described by Kick's law, that is, $P = Ch^2$, where P is the indenter load and h is the indenter penetration [21]. Furthermore, the load-depth curve obtained on bulk Si (100) and on the pillar using the Berkovich indenter are very similar, showing only a slight divergence near the splitting load. Similar trends were observed for TiN and CrN thin films, for which residual stresses were released during the pillar fabrication [6,18].

Figure 2b shows the splitting load as a function of the indenter angle for the three materials. In general, for a given diameter, the splitting load linearly increases for larger indenter angles As a matter of fact, the sharper indenter provokes a reduction of the splitting load because of the large stress

intensification. It is important to note here that the fact that the pillars have different diameters will lead to different splitting loads for the same material, according to eq. (1). However, the results here show that a similar linear trend, with very similar slopes, is observed for the splitting load as a function of indenter angle for the two pillar diameters that were used in the experiments (3 μm and 5 μm). As a result, there is a shift towards higher loads for the 5 μm pillars tested for TiN relative to the other materials with smaller pillar diameters (also reported in table I)

Table I summarizes the average splitting loads for the three different materials with the Berkovich tip. For the TiN pillars, which had two different radii, the splitting load for the smaller 3 μm-diameter pillars decreased from 28.42 ± 0.24 mN to 13.65 ± 0.49 mN. The γ coefficient in the table is that calculated from Ref. [6] after measuring the ratio of the elastic modulus to hardness (E/H) by nanoindentation experiments. Using these values, the fracture toughness (K_c) was computed using Equation (1).

Table I. *The fracture toughness (K_c) computed from the pillar splitting data obtained with the Berkovich indenter tip, and the parameters used in the computation. Note that for TiN, similar K_c values are found for two different pillar radii.*

Material	**Pillar radius (μm)**	**Splitting load (mN)**	***E/H* (-)**	**γ (-) (Berkovich)**	**K_c (MPa m$^{1/2}$)**
Si (100)	2.60 ± 0.01	16.14 ± 0.10	14.1 ± 0.9	0.25	0.96 ± 0.05
TiN	2.62 ± 0.07	28.42 ± 0.24	18.9 ± 1.1	0.34	2.28 ± 0.11
	1.58 ± 0.02	13.65 ± 0.49	18.9 ± 1.1	0.34	2.33 ± 0.08
CrN	1.59 ± 0.05	16.31 ± 0.65	13.9 ± 0.9	0.25	2.00 ± 0.05

The values of K_c given in Table I are in agreement with other measurements for Si (100), CrN and TiN using the pillar splitting technique [6,17,18], and they are also in agreement with values obtained using other techniques, i.e. single cantilever bending and double cantilever [15,17]. Specifically, Jaya *et al.* [15] reported a K_c equal to 1.00 ± 0.15 MPa $m^{1/2}$ for Si (100) using the single cantilever method, while Best *et al.* [17] reported a value of 3.33 ± 0.26 MPa $m^{1/2}$ for CrN using the double cantilever method.

As discussed in other papers [17], a possible explanation for differences between the pillar splitting method and the cantilever-based method could be the different amounts of FIB ion damage, specifically, it has been suggested that FIB ion damage may be more for FIB notched cantilevers [17]. It should also be noted that for TiN, the change of the pillar radius did not affect the measured value of K_c since the smaller pillar radius produces a reduction of the splitting load. The invariance of fracture toughness is due to the fact that that the grain size is significantly smaller than the pillar radius and indentation contact size. Some dependence of the splitting load on pillar radius could be expected when the pillar radius becomes comparable to the grain size.

Figure 3a,b shows examples of the cohesive zone finite element mesh used to compute the γ coefficient for the different material properties and indenter geometries. The symmetry of the three-sided indenter was used to minimize the number of elements required in the simulations resulting, in the six-fold symmetric model as shown in the figure. The two extreme cases of the Berkovich (65.30°) and cube corner tip (35.3°) are represented in Figures 3a and 3b, respectively.

Figure 3c shows the variation of γ with the material parameter E/H. The full symbols represent the CZ-FEM calculated γ coefficients for a Poisson ratio of 0.25. The results for the Berkovich tip are the same as those in Ref. [6], in which γ increases from 0.145 (E/H = 7.0) up to 0.4 for E/H equal to 31. A similar trend is observed for the other indenter geometries, with a shift to higher γ values for sharper indenters. These results are in good agreement with the analogous trend of the function $f(H)$ reported in

a Ref. [11], where *f(H)* is a constant term that relates the fracture toughness (K_c) to the applied load and the crack length during standard nanoindentation experiments using the Lawn–Evans–Marshall (LEM) model [8].

A first way to validate the CZ-FEM results is to recalculate the γ coefficient from the experimentally measured splitting loads, assuming that the "true" the fracture toughness K_c is that obtained using the Berkovich indenter (this was validated in a previous work, see Table I and Ref. [6]). Shown as the open symbols in Fig. 3c, the experimentally calculated values are in very good agreement with the finite element results. This is also shown in Figure 3d, where the variation of γ with indenter angle is plotted. Curiously, a very linear decrease in γ is observed for the range of indenter angles considered. A similar linear trend was reported by Jang and Pharr, who performed indentation experiments in Si (100) with different indenter tips [21]. Specifically, they found that the constant of proportionality α between K_c and the crack length linearly scales with the indenter angle [21], with a slope of about -0.08. It is worth noting that the slope extracted from linear fit (Figure 3d) is close to ~ -0.08, and thus in close agreement with the one that was found for α in a previous publication [21].

As a further validation, Figure 4 presents the calculated K_c values for all materials and indenter geometries, using the values of γ determined in the finite element simulations (Figures 3c,d). Note that the value of K_c is independent of the indenter angle. This is a very important result since it suggests that that γ is not too sensitive to frictional effects, which often become more pronounced for sharper indenters. Thus, cube-corner indenters, which induce cracking at much lower loads than Berkovich indenters, can be used effectively in pillar splitting experiments.

Indeed, there may be additional advantages from the use of sharper indenters in pillar splitting measurements. As discussed in a previous paper by Lawn *et al.* [22], the critical pillar diameter, *d*, for crack initiation/nucleation can be estimated from:

$$d = \sqrt{2\chi}\frac{K_{Ic}^2}{H^2} \quad (2)$$

where the coefficient χ is linearly dependent on indenter angle. Therefore, the use of a sharper indenter will reduce the minimum required pillar diameter to have crack initiation, and possibly extend the applicability of the technique to brittle intermetallics and maybe to high-temperature fracture toughness assessment.

Figure 3e shows the effects of Poisson ratio on the γ coefficient calculated for the Berkovich indenter. Here, Poisson's ratio has been varied from 0.20 to 0.30 for the *E/H* interval between 7 and 23, while it has been varied from 0 up to 0.40 for *E/H* equal to 31. Figure 3e interestingly shows a weaker dependence of Poisson's ratio on the calculated gamma for the *E/H* interval 7-23, while a larger effect is reported for *E/H* equal to 31. This is also observed for sharp indentation on bulk materials [11].

As a final validation of the experimental and modelling results, Table II reports a comparison of the measured and simulated splitting loads for all materials and indenter angles. The values are normalized with respect to the reference splitting load obtained (for each material) using the Berkovich indenter. The agreement between experiment and FEM simulation is generally very good, further demonstrating the potential utility of using sharper indenters to make fracture toughness measurements.

Table II. *Ratio between the splitting load of the Berkovich (65.3°) and other indenters calculated for different materials using the results from both cohesive zone finite element simulations and experiments.*

Material	$P_B/P_{55°}$ **(experiments)**	$P_B/P_{55°}$ **(CZ-FEM)**	$P_B/P_{45°}$ **(experiments)**	$P_B/P_{45°}$ **(CZ-FEM)**	P_B/P_{CC} **(experiments)**	P_B/P_{CC} **(CZ-FEM)**
Si (100)	1.48 ± 0.10	1.48	2.02 ± 0.08	2.01	2.77 ± 0.21	2.80

TiN	1.34 ± 0.12	1.37	1.64 ± 0.17	1.68	2.21 ± 0.18	2.23
CrN	1.32 ± 0.14	1.33	1.61 ± 0.10	1.63	2.31 ± 0.19	2.32

As a final point, we wish to comment on the choice of the most suitable constitutive model to be used in CZ-FEM simulations. Specifically, the standard volume-conserving von Mises plasticity model may be not appropriate for some materials that show inelastic densification during deformation (e.g., fused Silica and borosilicate glasses). In a recent paper by Bruns *et al.* [23], cohesive-zone finite element simulations that incorporate densification were used to explore the role played by densification on plasticity and cracking in fused silica, a material that is known to densify during indentation. Results show that the use of a Drucker-Prager Cap model for plasticity, which includes densification-hardening effects, gives good agreement between simulated and experimental load displacement curves obtained using indenters with several different angles. The simulations also suggest that, in comparison with the conventional von Mises model, there is lower extension of the plastic zone beneath the hardness impression and shorter cracks for the case of the Drucker-Prager model. As a consequence, the onset for cracking is shifted to larger loads for those materials that show a tendency to densify during indentation [23]. By extension, one may expected a similar behavior for the pillar indentation problem in fused silica or other materials that densify during indentation.

IV. Conclusions

It has been shown that measurement of the critical loads needed to split micro-pillars in conjunction with the results of cohesive zone finite element simulations can be used to effectively measure the fracture toughness of brittle materials at the micrometer scale. Very good agreement between experiments and simulations was observed, with a linear correlation between the splitting load and the indenter angle. We also find a linear relationship between the γ coefficient and the indenter angle for a wide range of E/H and Poisson's ratios.

The results presented here pave the way for the use of sharper indenters in the pillar splitting technique for micro-scale fracture toughness assessment. This is particularly relevant considering that most of the *in-situ* (in-SEM) fracture testing procedures are often performed using cube-corner indenters. Additionally, the use of sharp indenter tips could open new possibilities for testing brittle intermetallics, where the Berkovich indenter is not effective because it cannot induce cracking. For the same reason, the use of sharper tips could be particularly useful for high-temperature fracture assessment in ceramics, thus paving the way for further insights into the temperature dependence of the mechanical and fracture properties of advanced materials and coatings.

Acknowledgments

FIB sample preparation was performed at the interdepartmental laboratory of electron microscopy (LIME lab) of Roma TRE University, with the assistance of Daniele de Felicis. GMP's contributions to this work were supported by the National Science Foundation under grant number DMR-1427812.

List of figure captions

Figure 1. Effects of indenter geometry on pillar splitting. The upper row shows the geometry before splitting. The scale bars for Si and TiN are 5 μm, while for CrN and TiN they are 3 μm.

Figure 2. (a) Experimental results for pillar splitting of Si (100). The effects of the indenter geometry on the splitting load are highlighted. **b)** Average splitting load as a function of the indenter angle for each of the three materials.

Figure 3. (a,b) Finite element meshes used for the Berkovich and cube-corner tip**. (c)** The gamma coefficient vs E/H for different tip geometries. The full and empty symbols represent, respectively, the FEM simulations and the experimental data. **(d)** The gamma coefficient as a function of the indenter angle. Empty and full symbols represent the experimental and the CZ-FEM data, respectively. **(e)** Effects of Poisson ratio on the gamma coefficient for a Berkovich (65.3°) tip. Data are fitted using equation (2).

Figure 4. Measured fracture toughness of the three materials under investigation as a function of indenter angle. For a given material, no changes in toughness are observed for pillar diameters in the range of 3-5 μm.

References

1. Franssila S *Introduction to Microfabrication*; John Wiley & Sons Ltd, 2010.

2. Greer JR,De Hosson JTM. Plasticity in small-sized metallic systems: Intrinsic versus extrinsic size effect. *Prog. Mater. Sci.* 2011; 56: 654-724.

3. Artz E. Size effects in materials due to microstructural and dimensional constraints: a comparative review. *Acta Metall.* 1998; 46: 5611-5626.

4. Ghidelli M, S. Gravier, J.-J. Blandin et al. Extrinsic mechanical size effects in thin ZrNi metallic glass films. *Acta Mater.* 2015; 90: 232-241.

5. Ghidelli M, Idrissi H, Gravier S et al. Homogeneous flow and size dependent mechanical behavior in highly ductile Zr 65 Ni 35 metallic glass films. *Acta Mater.* 2017; 131: 246-259.

6. Sebastiani M, Johanns KE, Herbert EG et al. Measurement of fracture toughness by nanoindentation methods: Recent advances and future challenges. *Curr. Opin. Solid St. M.* 2015; 19: 324-333.

7. Jaya BN, Kirchlechner C,Dehm G. Can microscale fracture tests provide reliable fracture toughness values? A case study in silicon. *J. Mater. Res.* 2015; 30: 686-698.

8. Lawn BR, Evans A,Marshall D. Elastic/plastic indentation damage in ceramics: the median/radial crack system. *J. Am. Ceram. Soc.* 1980; 63: 574-581.

9. Cook RF,Pharr GM. Direct observation and analysis of indentation cracking in glasses and ceramics. *J. Am. Ceram. Soc.* 1990; 73: 787-817.

10. Johanns KE, Lee JH, Gao YF et al. An evaluation of the advantages and limitations in simulating indentation cracking with cohesive zone finite elements. *Model Simul. Mater. Sci.* 2014; 22: 015011.

11. Lee J, Gao Y, Johanns K et al. Cohesive interface simulations of indentation cracking as a fracture toughness measurement method for brittle materials. *Acta Mater.* 2012; 60: 5448-5467.

12. Riedl A, Daniel R, Stefenelli M et al. A novel approach for determining fracture toughness of hard coatings on the micrometer scale. *Scripta Mater.* 2012; 67: 708-711.

13. Kupka D, Huber N,Lilleodden E. A combined experimental-numerical approach for elasto-plastic fracture of individual grain boundaries. *J. Mech. Phys. Solids.* 2014; 64: 455-467.

14. Schaufler J, Schmid C, Durst K et al. Determination of the interfacial strength and fracture toughness of aC: H coatings by in-situ microcantilever bending. *Thin Solid Films.* 2012; 522: 480-484.

15. Jaya BN, Wheeler JM, Wehrs J et al. Microscale Fracture Behavior of Single Crystal Silicon Beams at Elevated Temperatures. *Nano Lett.* 2016; 16: 7597-7603.

16. Liu S, Raghavan R, Zeng XT et al. Compressive deformation and failure of CrAlN/Si3N4 nanocomposite coatings. *App. Phys. Lett.* 2014; 104: 081919.

17. Best JP, Zechner J, Wheeler JM et al. Small-scale fracture toughness of ceramic thin films: the effects of specimen geometry, ion beam notching and high temperature on chromium nitride toughness evaluation. *Philos. Mag.* 2016; 96: 3552-3569.

18. Sebastiani M, Johanns KE, Herbert EG et al. A novel pillar indentation splitting test for measuring fracture toughness of thin ceramic coatings. *Philos. Mag.* 2014; 95: 1928-1944.

19. Mughal MZ, Moscatelli R, Amanieu H-Y et al. Effect of lithiation on micro-scale fracture toughness of LixMn2O4 cathode. *Scripta Mater.* 2016; 116: 62-66.

20. Salvati E, Sui T, Lunt AJ et al. The effect of eigenstrain induced by ion beam damage on the apparent strain relief in FIB-DIC residual stress evaluation. *Mater. Design.* 2016; 92: 649-658.

21. Jang J-i,Pharr GM. Influence of indenter angle on cracking in Si and Ge during nanoindentation. *Acta Mater.* 2008; 56: 4458-4469.

22. Lawn B,Evans A. A model for crack initiation in elastic/plastic indentation fields. *J. Mater. Sci.* 1977; 12: 2195-2199.

23. Bruns S, Johanns KE, Rehman H et al. Constitutive modeling of indentation cracking in fused silica. *J. Am. Ceram. Soc.* 2017; 00: 1-13.

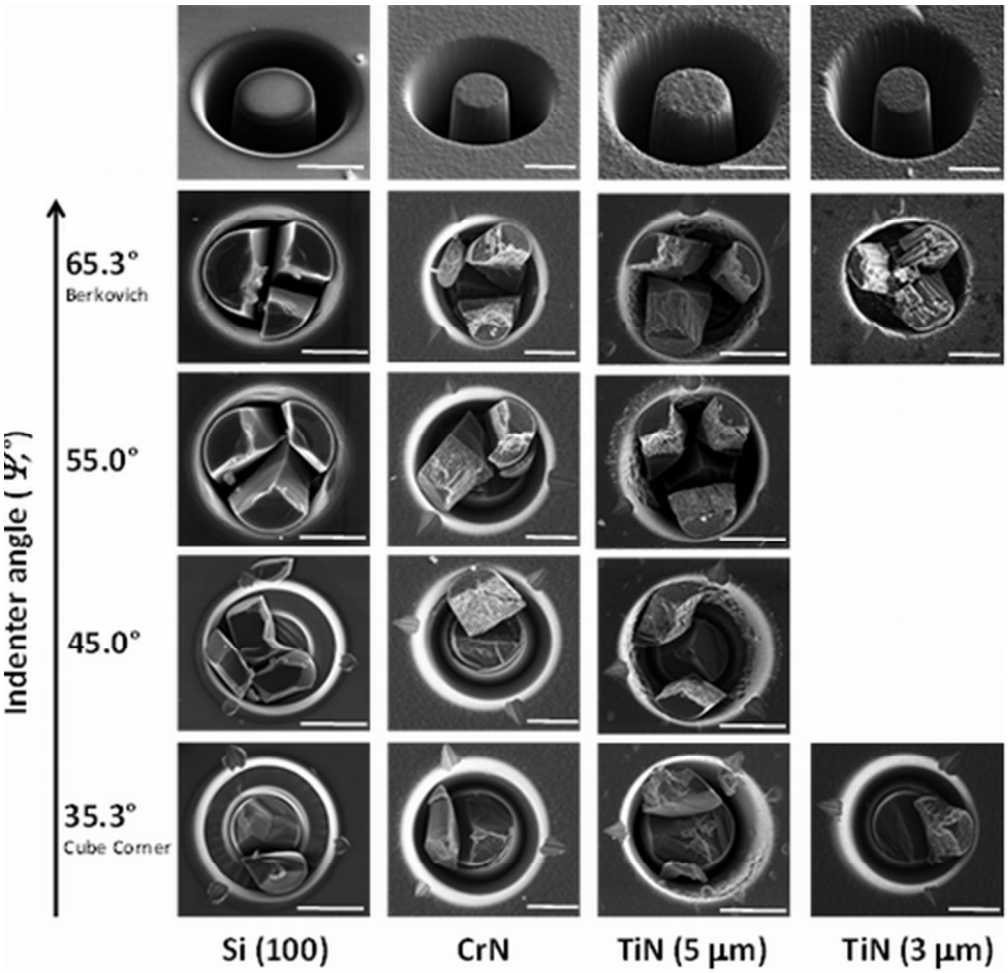

Figure 1. Effects of indenter geometry on pillar splitting. The upper row shows the geometry before splitting. The scale bars for Si and TiN are 5 um, while for CrN and TiN they are 3 um.

85x81mm (300 x 300 DPI)

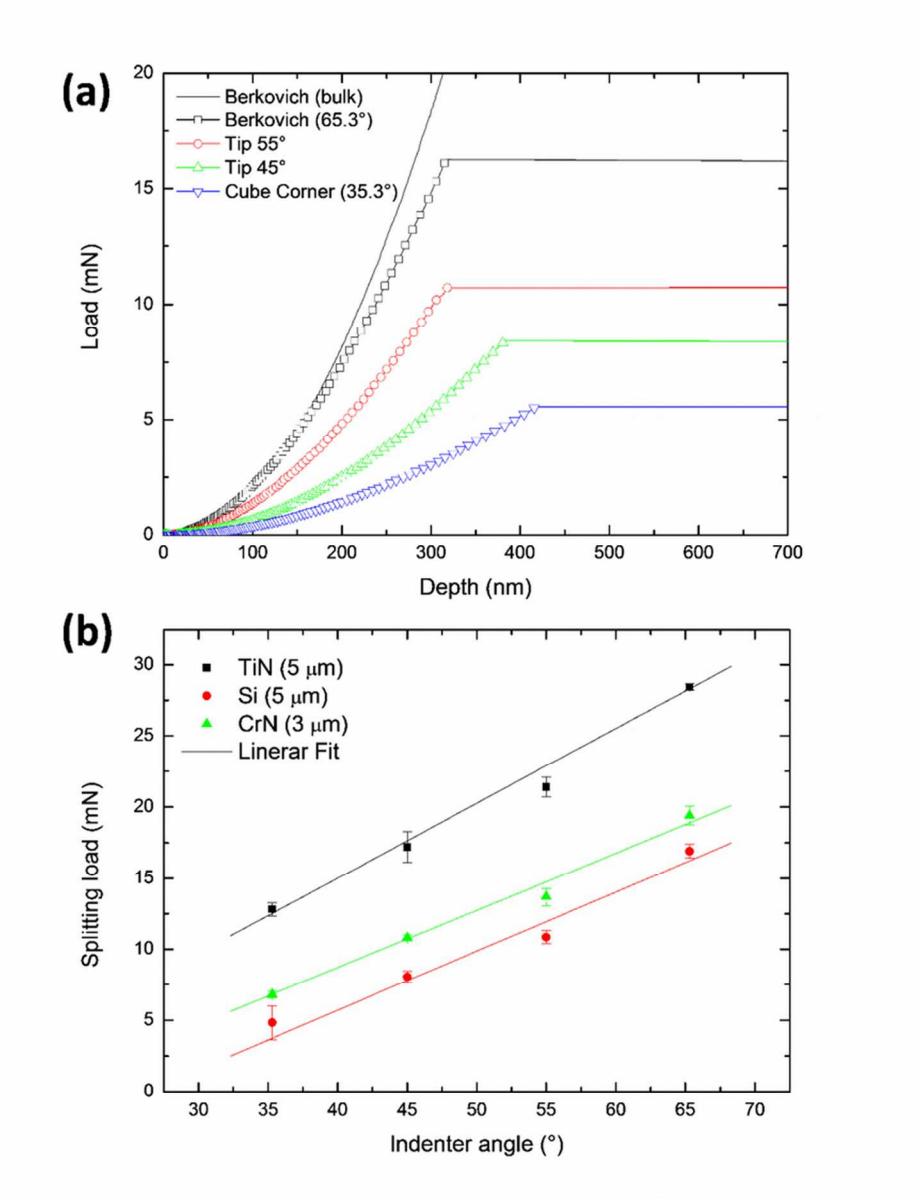

Figure 2. (a) Experimental results for pillar splitting of Si (100). The effects of the indenter geometry on the splitting load are highlighted. b) Average splitting load as a function of the indenter angle for each of the three materials.

85x111mm (300 x 300 DPI)

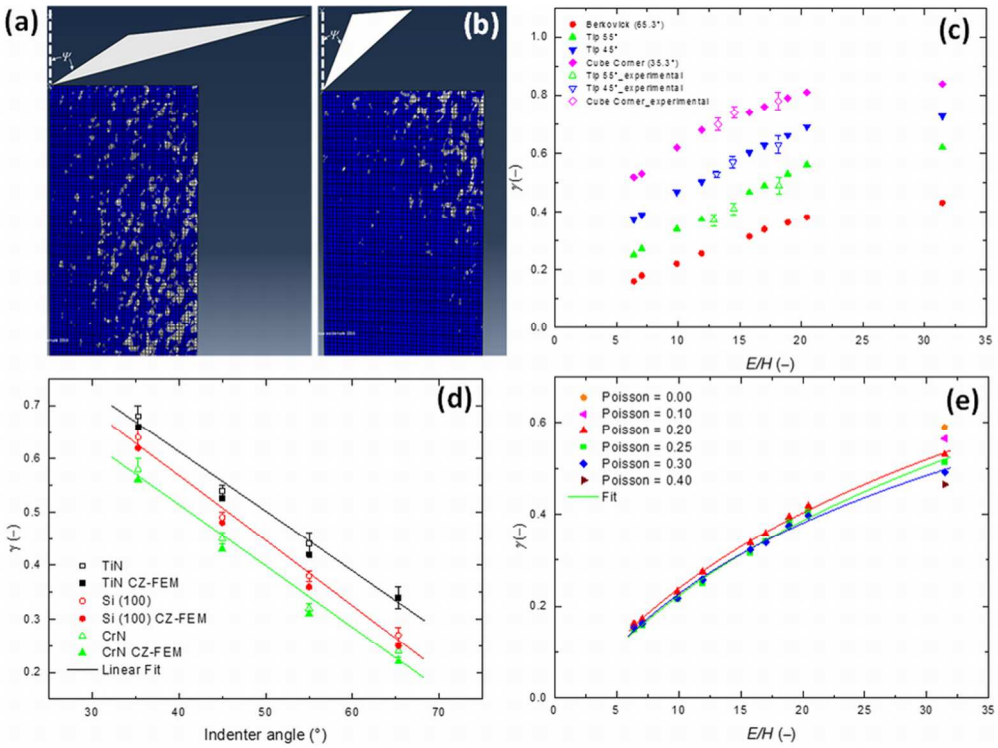

Figure 3. (a,b) Finite element meshes used for the Berkovich and cube-corner tip. (c) The gamma coefficient vs E/H for different tip geometries. The full and empty symbols represent, respectively, the FEM simulations and the experimental data. (d) The gamma coefficient as a function of the indenter angle. Empty and full symbols represent the experimental and the CZ-FEM data, respectively. (e) Effects of Poisson ratio on the gamma coefficient for a Berkovich (65.3°) tip. Data are fitted using equation (2).

85x63mm (300 x 300 DPI)

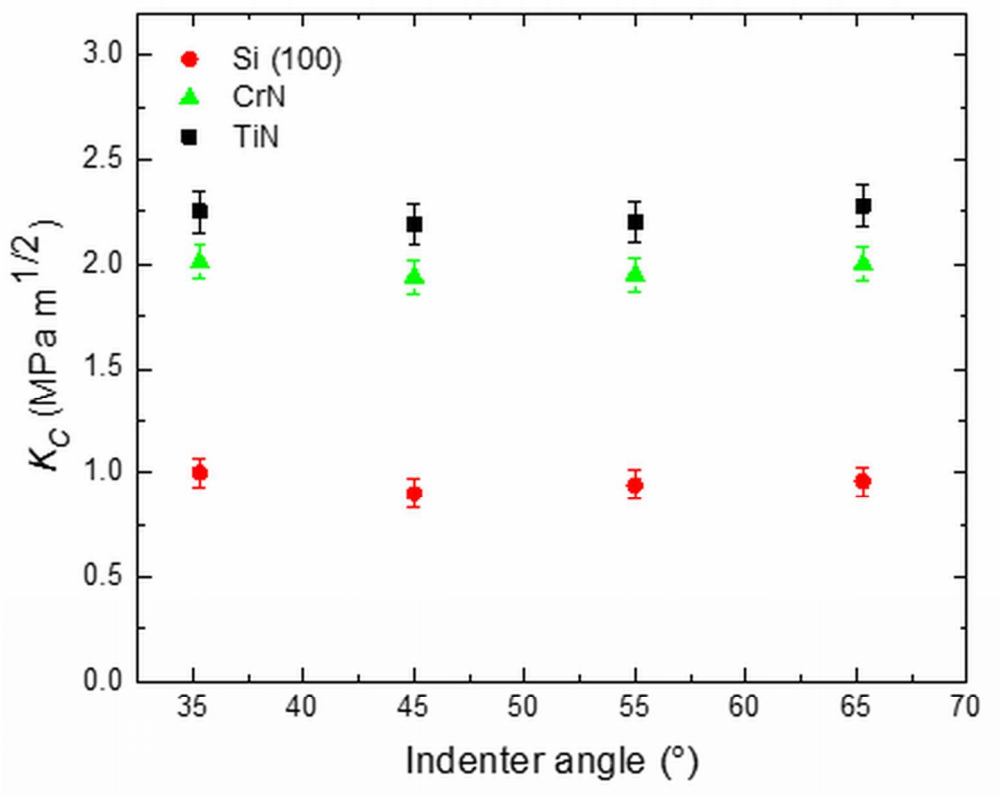

Figure 4. Measured fracture toughness of the three materials under investigation as a function of indenter angle. For a given material, no changes in toughness are observed for pillar diameters in the range of 3-5 μm.

85x67mm (300 x 300 DPI)